Photoionization and core resonances from range-separated time-dependent density-functional theory for open-shell states: Example of the lithium atom

Julien Toulouse, Karno Schwinn, Felipe Zapata, Antoine Levitt, Éric Cancès, Eleonora Luppi

Photoionization and core resonances from range-separated time-dependent density-functional theory for open-shell states: Example of the lithium atom

Julien Toulouse,[1, 2, ∗] Karno Schwinn,[1] Felipe Zapata,[3] Antoine Levitt,[4] Éric Cancès,[5] and Eleonora Luppi[1, †]

[1]*Laboratoire de Chimie Théorique, Sorbonne Université and CNRS, F-75005 Paris, France*
[2]*Institut Universitaire de France, F-75005 Paris, France*
[3]*Department of Physics, Lund University, Box 118, SE-221 00 Lund, Sweden*
[4]*Laboratoire de mathématiques d'Orsay, Université Paris-Saclay and CNRS, F-91405 Orsay, France*
[5]*CERMICS, École des Ponts and Inria Paris, 6 & 8 Avenue Blaise Pascal, 77455 Marne-la-Vallée, France*
(Dated: November 12, 2022)

We consider the calculations of photoionization spectra and core resonances of open-shell systems using range-separated time-dependent density-functional theory. Specifically, we use the time-dependent range-separated hybrid (TDRSH) scheme, combining a long-range Hartree-Fock (HF) exchange potential and kernel with a short-range potential and kernel from a local density-functional approximation, and the time-dependent locally range-separated hybrid (TDLRSH) scheme, which uses a local range-separation parameter. To efficiently perform the calculations, we formulate a spin-unrestricted linear-response Sternheimer approach in a non-orthogonal B-spline basis set and using appropriate frequency-dependent boundary conditions. We illustrate this approach on the Li atom, which suggests that TDRSH and TDLRSH are adequate simple methods for estimating single-electron photoionization spectra of open-shell systems.

I. INTRODUCTION

Adiabatic linear-response time-dependent density-functional theory (TDDFT) [1–4], using range-separated approximations [5–12], is recognized as a practical and reasonably accurate approach for calculating bound-state electronic excitations in many molecular systems (see, e.g., Refs. 13 and 14). A natural question is then whether these range-separated TDDFT methods can be also successfully extended from bound to continuum excitations in order to calculate for example photoionization spectra and resonances in atomic and molecular systems.

In Ref. 15, some of the present authors started to explore the merits of range-separated TDDFT for the calculation of photoionization spectra and showed that the so-called linear-response time-dependent range-separated hybrid (TDRSH) scheme [12, 16], combining a long-range Hartree-Fock (HF) exchange potential and kernel with a short-range potential and kernel from a local density-functional approximation, provides an adequate (single-electron) photoionization spectrum of the He atom. Technically, in Ref. 15, the continuum was described by the use of B-spline basis set within a computational box and the photoionization spectrum was straightforwardly calculated by diagonalization of the linear-response Casida equations (in the orthogonal occupied/virtual orbital basis) using zero boundary conditions at the edge of the box. In Ref. 17, the present authors extended this study to the Be atom and showed that the TDRSH scheme and a close variant, namely the time-dependent locally range-separated hybrid (TDLRSH) scheme, also give overall reasonable (single-electron) photoionization spectra for this system, with core resonances at approximately correct resonance energies, albeit with much too small resonance widths. To be able to

efficiently apply TDRSH and TDLRSH to the Be atom, in Ref. 17, we use a linear-response Sternheimer approach [18–26] (in the non-orthogonal B-spline basis) using appropriate frequency-dependent boundary conditions at the edge of the computational box.

The work of Ref. 17 was restricted to systems with closed-shell ground-state states. In the present work, we extend the theory of Ref. 17 to systems with open-shell ground-state states. For this, we provide equations for a general linear-response Sternheimer scheme (in a non-orthogonal basis set) within a spin-unrestricted formalism, and again with frequency-dependent boundary conditions at the edge of the computational box. As an illustration, we use this scheme to calculate photoionization spectra of the Li atom at the TDRSH and TDLRSH levels, we extract Fano parameters of some of the core resonances, and we compare with the standard time-dependent local-density approximation (TDLDA) and time-dependent Hartree-Fock (TDHF) methods.

The paper is organized as follows. In Section II, we review the range-separated hybrid (RSH) and locally range-separated hybrid (LRSH) schemes in a spin-unrestricted formalism, and give in some detail the linear-response spin-unrestricted Sternheimer equations including a nonlocal HF exchange kernel both in real space and in a general non-orthogonal basis set which, to the best of our knowledge, were never given in the literature. We also give some computational details for our specific implementation for the Li atom using a B-spline basis set. In Section III, we give and discuss the results obtained on the Li atom. We explain how to select an optimal range-separation parameter, we discuss the calculated photoionization spectra, and we analyze the core resonances. Section IV contains our conclusions.

∗ toulouse@lct.jussieu.fr
† eleonora.luppi@lct.jussieu.fr

II. THEORY AND COMPUTATIONAL METHOD

We work on the one-electron Hilbert space $L^2(\mathbb{R}^3_\Sigma, \mathbb{C})$ where $\mathbb{R}^3_\Sigma = \mathbb{R}^3 \times \Sigma$ and $\Sigma = \{\uparrow, \downarrow\}$ is the set of spin coordinates. We denote a space-spin electron coordinate as $\mathbf{x} = (\mathbf{r}, s) \in \mathbb{R}^3_\Sigma$. We use throughout a spin-unrestricted formalism. Unless otherwise indicated, Hartree atomic units are used in this work.

A. Range-separated hybrid scheme

In the range-separated hybrid (RSH) scheme [27], the spin-orbitals $\{\varphi_i\}$ and their associated energies $\{\varepsilon_i\}$ of an N-electron system are found from the self-consistent Schrödinger-type equation

$$\int_{\mathbb{R}^3_\Sigma} h[\gamma_0](\mathbf{x}, \mathbf{x}')\varphi_i(\mathbf{x}')\mathrm{d}\mathbf{x}' = \varepsilon_i\varphi_i(\mathbf{x}), \tag{1}$$

where $h[\gamma_0](\mathbf{x}, \mathbf{x}')$ is the nonlocal RSH Hamiltonian depending on the density matrix $\gamma_0(\mathbf{x}, \mathbf{x}') = \sum_{i=1}^N \varphi_i(\mathbf{x})\varphi_i^*(\mathbf{x}')$. The RSH Hamiltonian has the form, for a generic density matrix γ,

$$h[\gamma](\mathbf{x}, \mathbf{x}') = T(\mathbf{x}, \mathbf{x}') + \delta(\mathbf{x} - \mathbf{x}')v_{\mathrm{ne}}(\mathbf{r}) + v_{\mathrm{Hxc}}[\gamma](\mathbf{x}, \mathbf{x}'), \tag{2}$$

where $T(\mathbf{x}, \mathbf{x}')$ is the kinetic integral kernel such that $\int_{\mathbb{R}^3} T(\mathbf{x}, \mathbf{x}')\varphi_i(\mathbf{x}')\mathrm{d}\mathbf{x}' = -(1/2)\nabla^2_\mathbf{r}\varphi_i(\mathbf{x})$, and $v_{\mathrm{ne}}(\mathbf{r})$ is the nuclei-electron potential and $v_{\mathrm{Hxc}}[\gamma](\mathbf{x}, \mathbf{x}')$ is the Hartree-exchange-correlation potential. The expression of $v_{\mathrm{Hxc}}[\gamma](\mathbf{x}, \mathbf{x}')$ is

$$v_{\mathrm{Hxc}}[\gamma](\mathbf{x}, \mathbf{x}') = \delta(\mathbf{x} - \mathbf{x}')v_{\mathrm{H}}[\rho_\gamma](\mathbf{r}) + v_{\mathrm{x}}^{\mathrm{lr,HF}}[\gamma](\mathbf{x}, \mathbf{x}')$$
$$+ \delta(\mathbf{x} - \mathbf{x}')v_{\mathrm{xc}}^{\mathrm{sr}}[\rho_\gamma](\mathbf{x}), \tag{3}$$

containing the local Hartree potential

$$v_{\mathrm{H}}[\rho_\gamma](\mathbf{r}) = \int_{\mathbb{R}^3_\Sigma} \rho_\gamma(\mathbf{x}')w_{\mathrm{ee}}(\mathbf{r}, \mathbf{r}')\mathrm{d}\mathbf{x}', \tag{4}$$

written with the spin-resolved density $\rho_\gamma(\mathbf{x}) = \gamma(\mathbf{x}, \mathbf{x})$ and the Coulomb electron-electron interaction $w_{\mathrm{ee}}(\mathbf{r}, \mathbf{r}') = 1/|\mathbf{r} - \mathbf{r}'|$, the nonlocal long-range (lr) HF exchange potential

$$v_{\mathrm{x}}^{\mathrm{lr,HF}}[\gamma](\mathbf{x}, \mathbf{x}') = -\gamma(\mathbf{x}, \mathbf{x}')w_{\mathrm{ee}}^{\mathrm{lr}}(\mathbf{r}, \mathbf{r}'), \tag{5}$$

written with the long-range electron-electron interaction [28]

$$w_{\mathrm{ee}}^{\mathrm{lr}}(\mathbf{r}, \mathbf{r}') = \frac{\mathrm{erf}(\mu|\mathbf{r} - \mathbf{r}'|)}{|\mathbf{r} - \mathbf{r}'|}, \tag{6}$$

with $\mu = \tilde{\mu}/a_0$ where $a_0 = 1$ a.u. is the Bohr radius and $\tilde{\mu} \in [0, +\infty)$ is the adimensional range-separation parameter, and the local complementary short-range (sr) exchange-correlation potential $v_{\mathrm{xc}}^{\mathrm{sr}}[\rho_\gamma](\mathbf{x})$. For the latter term, we use in this work the LDA

$$v_{\mathrm{xc}}^{\mathrm{sr}}[\rho_\gamma](\mathbf{r}, s) = \left.\frac{\partial \bar{e}_{\mathrm{xc,UEG}}^{\mathrm{sr}}(\rho_\uparrow, \rho_\downarrow, \mu)}{\partial \rho_s}\right|_{\substack{\rho_\uparrow = \rho_\gamma(\mathbf{r},\uparrow)\\\rho_\downarrow = \rho_\gamma(\mathbf{r},\downarrow)}}, \tag{7}$$

where $\bar{e}_{\mathrm{xc,UEG}}^{\mathrm{sr}}(\rho_\uparrow, \rho_\downarrow, \mu)$ is the spin-dependent complementary short-range exchange-correlation energy density of the uniform-electron gas (UEG), as parametrized in Ref. 29.

In the locally range-separated hybrid (LRSH) scheme 17, 30–34, the range-separation parameter μ in Eqs. (6) and (7) is replaced by a function of position $\mathbf{r} \mapsto \mu(\mathbf{r})$. The long-range electron-electron interaction in Eq. (6) now becomes [32]

$$w_{\mathrm{ee}}^{\mathrm{lr}}(\mathbf{r}, \mathbf{r}') = \frac{1}{2}\left[\frac{\mathrm{erf}(\mu(\mathbf{r})|\mathbf{r} - \mathbf{r}'|)}{|\mathbf{r} - \mathbf{r}'|} + \frac{\mathrm{erf}(\mu(\mathbf{r}')|\mathbf{r} - \mathbf{r}'|)}{|\mathbf{r} - \mathbf{r}'|}\right]. \tag{8}$$

Following Ref. 30, we choose $\mu(\mathbf{r})$ as

$$\mu(\mathbf{r}) = \frac{\tilde{\mu}}{2}\frac{|\nabla\rho(\mathbf{r})|}{\rho(\mathbf{r})}, \tag{9}$$

where again $\tilde{\mu} \in [0, +\infty)$ is the adimensional range-separation parameter and we take $\rho(\mathbf{r})$ as the fixed spin-unrestricted Hartree-Fock (UHF) ground-state density.

B. Linear-response Sternheimer equations in real space

We consider a time-dependent perturbation potential of the form

$$v_{\mathrm{ext}}(\mathbf{r}, t) = \left[v_{\mathrm{ext}}(\mathbf{r})e^{-\mathrm{i}\omega t} + v_{\mathrm{ext}}(\mathbf{r})e^{+\mathrm{i}\omega t}\right]e^{\eta t}, \tag{10}$$

where $v_{\mathrm{ext}}(\mathbf{r}) = \mathbf{r} \cdot \mathcal{E}\mathbf{e}$ is the electric-dipole interaction ($\mathcal{E}$ is the amplitude of the electric field and $\mathbf{e}$ is its unit polarization vector), $\omega \geq 0$ is the frequency, and $e^{\eta t}$ is an adiabatic switching factor with a small parameter $\eta > 0$. Following the same steps as in Ref. 17, it can be shown that the Fourier components at frequencies $\pm\omega + \mathrm{i}\eta$ of the first-order change of the occupied spin-orbital φ_i, namely $\psi_i^{(+)}$ and $\psi_i^{(-)}$, are given by the following TDRSH or TDLRSH Sternheimer equations

$$(\pm\omega + \mathrm{i}\eta + \varepsilon_i)\,\psi_i^{(\pm)}(\mathbf{x}_1, \omega) = \int_{\mathbb{R}^3_\Sigma} h[\gamma_0](\mathbf{x}_1, \mathbf{x}_1')\psi_i^{(\pm)}(\mathbf{x}_1', \omega)\mathrm{d}\mathbf{x}_1'$$
$$+ \int_{\mathbb{R}^9_\Sigma} f_{\mathrm{Hxc}}[\gamma_0](\mathbf{x}_1, \mathbf{x}_1'; \mathbf{x}_2, \mathbf{x}_2')\gamma^{(\pm)}(\mathbf{x}_2, \mathbf{x}_2', \omega)\varphi_i(\mathbf{x}_1')\mathrm{d}\mathbf{x}_1'\mathrm{d}\mathbf{x}_2\mathrm{d}\mathbf{x}_2' + v_{\mathrm{ext}}^{(1)}(\mathbf{r}_1)\varphi_i(\mathbf{x}_1), \tag{11}$$

with the first-order perturbation potential $v_{\mathrm{ext}}^{(1)}(\mathbf{r}) = \mathbf{r} \cdot \mathbf{e}$, the first-order changes of the density matrix

$$\gamma^{(\pm)}(\mathbf{x}, \mathbf{x}', \omega) = \sum_{i=1}^N \left[\psi_i^{(\pm)}(\mathbf{x}, \omega)\varphi_i^*(\mathbf{x}') + \varphi_i(\mathbf{x})\psi_i^{(\mp)*}(\mathbf{x}', \omega)\right], \tag{12}$$

and the Hartree-exchange-correlation kernel

$$f_{\mathrm{Hxc}}[\gamma_0](\mathbf{x}_1, \mathbf{x}_1'; \mathbf{x}_2, \mathbf{x}_2') = \delta(\mathbf{x}_1 - \mathbf{x}_1')\delta(\mathbf{x}_2 - \mathbf{x}_2')f_{\mathrm{H}}(\mathbf{r}_1, \mathbf{r}_2)$$
$$+ f_{\mathrm{H}}^{\mathrm{lr,HF}}(\mathbf{x}_1, \mathbf{x}_1'; \mathbf{x}_2, \mathbf{x}_2') + \delta(\mathbf{x}_1 - \mathbf{x}_1')\delta(\mathbf{x}_2 - \mathbf{x}_2')f_{\mathrm{xc}}^{\mathrm{sr}}[\rho_{\gamma_0}](\mathbf{x}_1, \mathbf{x}_2), \tag{13}$$

where $f_{\mathrm{H}}(\mathbf{r}_1, \mathbf{r}_2) = w_{\mathrm{ee}}(\mathbf{r}_1, \mathbf{r}_2)$ is the Hartree kernel, $f_{\mathrm{H}}^{\mathrm{lr,HF}}(\mathbf{x}_1, \mathbf{x}_1'; \mathbf{x}_2, \mathbf{x}_2') = -\delta(\mathbf{x}_1 - \mathbf{x}_2)\delta(\mathbf{x}_1' - \mathbf{x}_2')w_{\mathrm{ee}}^{\mathrm{lr}}(\mathbf{r}_1, \mathbf{r}_1')$ is the nonlocal HF exchange kernel, and $f_{\mathrm{xc}}^{\mathrm{sr}}[\rho_{\gamma_0}](\mathbf{x}_1, \mathbf{x}_2)$ is the short-range exchange-correlation kernel, which for the LDA [Eq. (7)] takes the local form

$$f_{\mathrm{xc}}^{\mathrm{sr}}[\rho_{\gamma_0}](\mathbf{r}_1, s_1, \mathbf{r}_2, s_2) =$$

$$\delta(\mathbf{r}_1 - \mathbf{r}_2) \left. \frac{\partial^2 \bar{e}_{\mathrm{xc,UEG}}^{\mathrm{sr}}(\rho_\uparrow, \rho_\downarrow, \mu)}{\partial \rho_{s_1} \partial \rho_{s_2}} \right|_{\substack{\rho_\uparrow = \rho_{\gamma_0}(\mathbf{r}_1, \uparrow) \\ \rho_\downarrow = \rho_{\gamma_0}(\mathbf{r}_1, \downarrow)}} . \quad (14)$$

The photoexcitation/photoionization cross section can then be calculated as [24]

$$\sigma(\omega) = \lim_{\eta \to 0^+} \frac{4\pi\omega}{c} \mathrm{Im}[\alpha(\omega + i\eta)], \quad (15)$$

where $c = 137.036$ a.u. is the speed of light and $\alpha(\omega)$ is the spherically averaged dipole polarizability given by

$$\alpha(\omega + i\eta) = -\frac{1}{3} \sum_{a \in \{x,y,z\}} \int_{\mathbb{R}^3_\Sigma} (\mathbf{r} \cdot \mathbf{u}_a) \, \rho^{(+)}(\mathbf{x}, \omega) d\mathbf{x}, \quad (16)$$

where $\mathbf{u}_a$ is the unit vector along the direction a and $\rho^{(+)}(\mathbf{x}, \omega) = \gamma^{(+)}(\mathbf{x}, \mathbf{x}, \omega)$.

C. Linear-response Sternheimer equations in a basis set

Let us introduce now a finite (non-orthogonal) spatial basis set on a domain $\Omega \subset \mathbb{R}^3$, i.e. $\{\chi_\nu\}_{\nu=1,\ldots,M} \subset H^1(\Omega, \mathbb{C})$ (where H^1 is the first-order Sobolev space), made of M basis functions to expand the occupied spin-orbitals

$$\varphi_j(\mathbf{r}, s) = \delta_{s_j, s} \sum_{\nu=1}^M c_{j\nu}\chi_\nu(\mathbf{r}), \quad (17)$$

where $s_j \in \Sigma$ is the spin of the spin-orbital j, and their first-order changes

$$\psi_j^{(\pm)}(\mathbf{r}, s, \omega) = \delta_{s_j, s} \sum_{\nu=1}^M c_{j\nu}^{(\pm)}(\omega)\chi_\nu(\mathbf{r}), \quad (18)$$

where $c_{j\nu}$ and $c_{j\nu}^{(\pm)}(\omega)$ are (generally complex-valued) coefficients labeled with the composite index $j\nu \equiv (j, \nu) \in [\![1, N]\!] \times [\![1, M]\!]$. Integrating Eq. (11) against a basis function χ_μ^*, and using the expansions of Eqs. (17) and (18), leads to the basis-set Sternheimer equations in the following block matrix form

$$\begin{pmatrix} \Lambda(\omega) & \mathbf{B} \\ \mathbf{B}^* & \Lambda(-\omega)^* \end{pmatrix} \begin{pmatrix} \mathbf{c}^{(+)}(\omega) \\ \mathbf{c}^{(-)}(\omega)^* \end{pmatrix} = -\begin{pmatrix} \mathbf{V} \\ \mathbf{V}^* \end{pmatrix}, \quad (19)$$

which must be solved at each given frequency ω for $\mathbf{c}^{(+)}(\omega)$ and $\mathbf{c}^{(-)}(\omega)^*$ which are the column vectors of components $c_{j\nu}^{(+)}(\omega)$ and $c_{j\nu}^{(-)}(\omega)^*$, respectively. In Eq. (19), $\mathbf{V}$ is the column vector of components $V_{i\mu} = \mathbf{e} \cdot \sum_{\nu=1}^M \mathbf{d}_{\mu,\nu}c_{i\nu}$ where $\mathbf{d}_{\mu,\nu} =$

$\int_\Omega \chi_\mu^*(\mathbf{r})\mathbf{r}\chi_\nu(\mathbf{r})d\mathbf{r}$ are the dipole-moment integrals, and $\Lambda(\pm\omega)$ and $\mathbf{B}$ are square matrices with elements

$$\Lambda_{i\mu, j\nu}(\pm\omega) = \delta_{i,j}\left(h_{i,\mu,\nu}(\pm\omega) - (\varepsilon_i \pm \omega + i\eta)S_{\mu,\nu}\right)$$

$$+ \sum_{\lambda=1}^M \sum_{\sigma=1}^M c_{i\sigma}c_{j\lambda}^* F_{\mu,\lambda,\sigma,\nu}^{s_i, s_j}, \quad (20)$$

and

$$B_{i\mu, j\nu} = \sum_{\lambda=1}^M \sum_{\sigma=1}^M c_{i\sigma}c_{j\lambda}F_{\mu,\nu,\sigma,\lambda}^{s_i, s_j}. \quad (21)$$

In Eq. (20), $S_{\mu,\nu} = \int_\Omega \chi_\mu^*(\mathbf{r})\chi_\nu(\mathbf{r})d\mathbf{r}$ are the overlap integrals over the basis functions, and $h_{i,\mu,\nu}(\pm\omega)$ are the matrix elements of the RSH or LRSH Hamiltonian

$$h_{i,\mu,\nu}(\pm\omega) = t_{i,\mu,\nu}(\pm\omega) + v_{\mu,\nu} \quad (22)$$

$$+ \sum_{\lambda=1}^M \sum_{\sigma=1}^M \left(P_{\sigma,\lambda}w_{\mu,\lambda,\nu,\sigma} - P_{\sigma,\lambda}^{s_i}w_{\mu,\lambda,\sigma,\nu}^{\mathrm{lr}}\right) + v_{\mu,\nu}^{\mathrm{sr}, s_i},$$

where $t_{i,\mu,\nu}(\pm\omega)$ are the kinetic integrals

$$t_{i,\mu,\nu}(\pm\omega) = \frac{1}{2} \int_\Omega \nabla\chi_\mu^*(\mathbf{r}) \cdot \nabla\chi_\nu(\mathbf{r})d\mathbf{r} \quad (23)$$

$$- \frac{1}{2} \int_{\partial\Omega^2} \chi_\mu^*(\mathbf{r})K_i(\mathbf{r}, \mathbf{r}'; \pm\omega)\chi_\nu(\mathbf{r}')d\mathbf{r}d\mathbf{r}',$$

where $K_i(\mathbf{r}, \mathbf{r}'; \pm\omega)$ is the Dirichlet-to-Neumann kernel imposing Robin boundary conditions on the surface $\partial\Omega$ [17], $v_{\mu,\nu} = \int_\Omega \chi_\mu^*(\mathbf{r})v_{\mathrm{ne}}(\mathbf{r})\chi_\nu(\mathbf{r})d\mathbf{r}$ are the nuclei-electron integrals, $P_{\sigma,\lambda} = \sum_{j=1}^N c_{j\sigma}c_{j\lambda}^*$ are the elements of the total density matrix, $P_{\sigma,\lambda}^{s_i} = \sum_{j=1}^N \delta_{s_j, s_i}c_{j\sigma}c_{j\lambda}^*$ are the elements of the density matrix of spin s_i, $w_{\mu,\lambda,\nu,\sigma} = \int_{\Omega^2} \chi_\mu^*(\mathbf{r}_1)\chi_\lambda^*(\mathbf{r}_2)w_{\mathrm{ee}}(\mathbf{r}_1, \mathbf{r}_2)\chi_\nu(\mathbf{r}_1)\chi_\sigma(\mathbf{r}_2)d\mathbf{r}_1d\mathbf{r}_2$ and $w_{\mu,\lambda,\sigma,\nu}^{\mathrm{lr}} = \int_{\Omega^2} \chi_\mu^*(\mathbf{r}_1)\chi_\lambda^*(\mathbf{r}_2)w_{\mathrm{ee}}^{\mathrm{lr}}(\mathbf{r}_1, \mathbf{r}_2)\chi_\sigma(\mathbf{r}_1)\chi_\nu(\mathbf{r}_2)d\mathbf{r}_1d\mathbf{r}_2$ are the Coulombic and long-range two-electron integrals, respectively, and $v_{\mu,\nu}^{\mathrm{sr}, s_i} = \int_\Omega \chi_\mu^*(\mathbf{r})v_{\mathrm{xc}}^{\mathrm{sr}}[\rho_{\gamma_0}](\mathbf{r}, s_i)\chi_\nu(\mathbf{r})d\mathbf{r}$ are the short-range exchange-correlation potential integrals. In Eqs. (20) and (21), $F_{\mu,\lambda,\sigma,\nu}^{s_i, s_j}$ comes from the matrix elements of the Hartree-exchange-correlation kernel $f_{\mathrm{Hxc}}[\gamma_0]$,

$$F_{\mu,\lambda,\sigma,\nu}^{s_i, s_j} = w_{\mu,\lambda,\sigma,\nu} - \delta_{s_i, s_j}w_{\mu,\lambda,\nu,\sigma}^{\mathrm{lr}} + f_{\mu,\lambda,\sigma,\nu}^{\mathrm{sr}, s_i, s_j}, \quad (24)$$

where $f_{\mu,\lambda,\sigma,\nu}^{\mathrm{sr}, s_i, s_j}$ are the short-range exchange-correlation kernel integrals

$$f_{\mu,\lambda,\sigma,\nu}^{\mathrm{sr}, s_i, s_j} =$$

$$\int_{\Omega^2} \chi_\mu^*(\mathbf{r}_1)\chi_\lambda^*(\mathbf{r}_2)f_{\mathrm{xc}}^{\mathrm{sr}}[\rho_{\gamma_0}](\mathbf{r}_1, s_i, \mathbf{r}_2, s_j)\chi_\sigma(\mathbf{r}_1)\chi_\nu(\mathbf{r}_2)d\mathbf{r}_1d\mathbf{r}_2.$$

$$(25)$$

Finally, in the basis set, the dipole polarizability takes the form

$$\alpha(\omega + i\eta) =$$

$$-\frac{1}{3} \sum_{a \in \{x,y,z\}} \sum_{\mu=1}^M \sum_{\nu=1}^M \left(P_{\mu,\nu}^{(+)}(\omega)\mathbf{d}_{\nu,\mu} + P_{\mu,\nu}^{(-)}(\omega)^*\mathbf{d}_{\nu,\mu}^*\right) \cdot \mathbf{u}_a, \quad (26)$$

where $P_{\mu,\nu}^{(\pm)}(\omega) = \sum_{i=1}^N c_{i\mu}^{(\pm)}(\omega)c_{i\nu}^*$.

D. Computational details

We apply the present theory to the Li atom ($N = 3$) in the ground-state configuration 1s²2s. We use a dipole interaction with a z-polarized electric field, i.e. $v_{\text{ext}}^{(1)} = \mathbf{r} \cdot \mathbf{u}_z$. The occupied spin-orbitals are of symmetry s ($\ell_i = 0$, $m_i = 0$) and the perturbed spin-orbitals are of symmetry p_z ($\ell = 1$, $m = 0$).

Just like in Ref. 17, we expand the radial parts of orbitals in a basis set of $M_s = 50$ B-spline functions [35, 36] of order $k_s = 8$, using a constant spatial grid spacing and a maximal radius of $r_{\text{max}} = 25$ bohr. The Robin boundary-condition term in Eq. (23) takes a simple radial local form, identical to the one used for the Be atom in Ref. 17. We use $\eta = 0$ to avoid artificially broadening of the resonances.

III. RESULTS AND DISCUSSION

We now show and discuss the results on the Li atom.

A. Orbital energies

Figure 1 shows the RSH and LRSH $1s_\uparrow$, $1s_\downarrow$ and $2s_\uparrow$ spin-orbital energies as a function of the adimensional range-separation parameter $\tilde{\mu}$. Also indicated are the opposite of the experimental IP (-5.392 eV) [37] and of the $1s_\uparrow$ ionization edge (corresponding to the two-electron state 1s2s ^{1}S, -66.31 eV) [38] and $1s_\downarrow$ ionization edge (corresponding to the two-electron state 1s2s ^{3}S, -64.41 eV) [38], as well as the Kohn-Sham (KS) exact exchange (EXX) $1s_\uparrow$, $1s_\downarrow$, and $2s_\uparrow$ spin-orbital energies (-55.94 eV, -67.18 eV, and -5.342 eV, respectively) [39] and the exact KS $1s_\uparrow$ spin-orbital energy (-55.97 eV [39]). According to spin-unrestricted KS theory [40, 41], the exact KS $2s_\uparrow$ spin-orbital energy must be equal to the opposite of the exact IP and the exact KS $1s_\downarrow$ spin-orbital energy must be equal to the opposite of the exact $1s_\downarrow$ ionization edge. As for the He atom [15], the KS EXX spin-orbital energies are rather close to the exact KS spin-orbital energies.

Let us first discuss the $2s_\uparrow$ spin-orbital energy. At $\tilde{\mu} = 0$, both RSH and LRSH reduce to standard KS, and give a far too high $2s_\uparrow$ spin-orbital energy (by more than 2 eV) due to the well-known self-interaction error of LDA. For $\tilde{\mu} \to \infty$, both RSH and LRSH reduce to standard HF, which gives a $2s_\uparrow$ spin-orbital energy very close to the opposite of the exact IP (error of only about 0.04 eV). Starting from $\tilde{\mu} = 0$, increasing $\tilde{\mu}$ reduces the self-interaction error in the short-range LDA exchange-correlation functional, and the $2s_\uparrow$ spin-orbital energy essentially reaches its HF value at around $\tilde{\mu} \approx 0.25$ for RSH and $\tilde{\mu} \approx 1$ for LRSH.

Let us now focus on the $1s_\uparrow$ and $1s_\downarrow$ spin-orbital energies. Both RSH and LRSH give very small energy splittings between the $1s_\uparrow$ and $1s_\downarrow$ spin-orbitals (at most about 0.5 eV for large $\tilde{\mu}$), in comparison with the energy splitting obtained with the exact KS (8.4 eV) and with the experimental ionization edges (1.9 eV). Again, at $\tilde{\mu} = 0$, RSH and LRSH reduce to standard KS, and give way too high $1s_\uparrow$ and $1s_\downarrow$ spin-orbital energies due to the use of the LDA.

For $\tilde{\mu} \to \infty$, when RSH and LRSH reduce to standard HF, we obtain $1s_\uparrow$ and $1s_\downarrow$ spin-orbital energies that are too low compared to the experimental ionization edges by about 1.6 and 3.0 eV, respectively. With the present approximations for the short-range exchange-correlation potential and kernel, the RSH and LRSH ionization energies correspond to the opposite of the occupied spin-orbital energies, and are identical to the TDRSH and TDLRSH ionization energies, respectively. In the philosophy of the so-called optimally tuned range-separated hybrids [8, 42, 43], in order to obtain correct ionization energies in TDRSH or TDLRSH, it is thus appropriate to choose the optimal adimensional range-separation parameter $\tilde{\mu}$ so that the RSH or LRSH spin-orbital energies are as close as possible to the opposite of the experimental ionization energies. Concretely, since we focus in the work on core excitations, we choose the optimal $\tilde{\mu}$ so as to symmetrically minimize the error in the $1s_\uparrow$ spin-orbital energy and the error in the $1s_\downarrow$ spin-orbital energy. This gives optimal adimensional range-separation parameters of $\tilde{\mu}_{\text{RSH}} = 1.431$ for RSH and $\tilde{\mu}_{\text{LRSH}} = 0.560$ for LRSH.

B. Photoionization spectrum

Figure 2 reports the photoionization cross section calculated by TDLDA, TDHF, TDRSH, and TDLRSH (using the optimal adimensional range-separation parameters determined in Section III A).

The TDLDA photoionization spectrum starts at a too low ionization threshold and the cross section is zero at the threshold, in agreement with the Wigner-threshold law [44, 45] for potentials lacking a long-range attractive $-1/r$ Coulomb tail. At the scale of the plot, the TDLDA $1s_\uparrow$ and $1s_\downarrow$ ionization edges are superimposed and occur at a much too low energy. The TDLDA photoionization spectrum contains only the two first $1s_\uparrow \to 2p_\uparrow$ and $1s_\downarrow \to 2p_\downarrow$ core resonances, the other core single-excited resonances (involving the orbitals 3p, 4p, etc.) having dissolved into the continuum beyond the 1s ionization edge.

The TDHF photoionization spectrum starts at an ionization threshold very close to the exact value, and the cross section is not zero at the threshold. Again, at the scale of the plot, the TDHF $1s_\uparrow$ and $1s_\downarrow$ ionization edges are almost superimposed and occur at a too high energy. In contrast to TDLDA, the TDHF photoionization spectrum contains not only the $1s_\uparrow \to 2p_\uparrow$ and $1s_\downarrow \to 2p_\downarrow$ core resonances, but also two intertwined series of single-excited core resonances to Rydberg states ($1s_\uparrow \to 3p_\uparrow$, $1s_\uparrow \to 4p_\uparrow$, etc., and $1s_\downarrow \to 3p_\downarrow$, $1s_\downarrow \to 4p_\downarrow$, etc.) converging toward the $1s_\uparrow$ and $1s_\downarrow$ ionization edges, respectively.

The TDRSH and TDLRSH photoionization spectra (using the optimal adimensional range-separation parameters determined in Section III A) display roughly the same features. They both start very close to the exact ionization threshold. For both TDRSH and TDLRSH, the $1s_\uparrow$ and $1s_\downarrow$ ionization edges (which are not resolved at the scale of the plot) occur near the experimental ionization edges, as expected since the adimensional range-separation parameter had been adjusted for this purpose. Similar to TDHF, both the TDRSH and
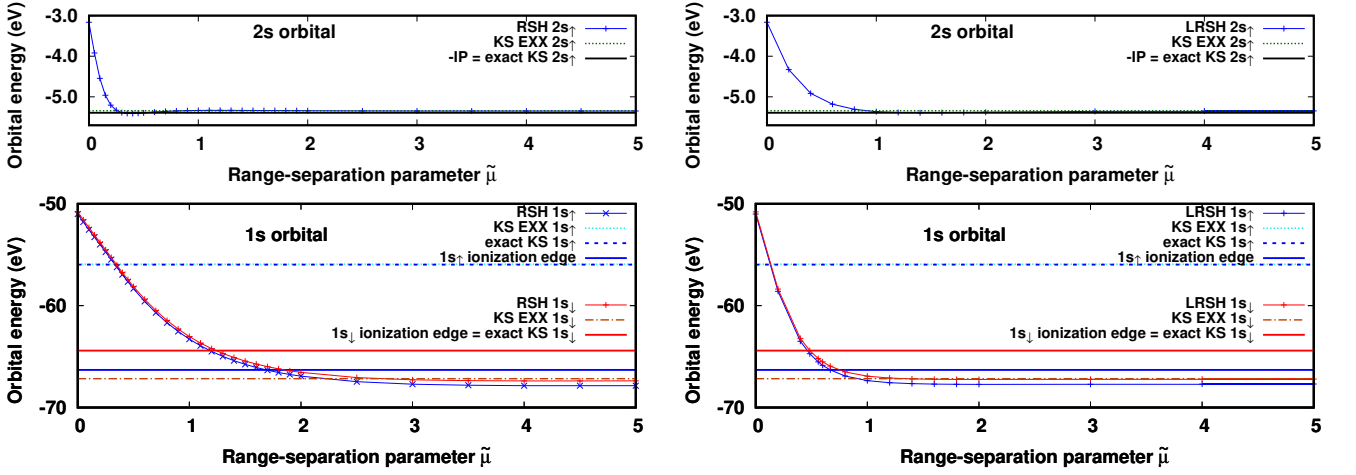
FIG. 1. RSH and LRSH $1s_\uparrow$, $1s_\downarrow$ and $2s_\uparrow$ spin-orbital energies of the Li atom as a function of the adimensional range-separation parameter $\tilde{\mu}$. As references, the opposite of the experimental IP (-5.392 eV) [37] and of the $1s_\uparrow$ ionization edge (corresponding to the state $1s2s$ ^{1}S, -66.31 eV) [38] and $1s_\downarrow$ ionization edge (corresponding to the state $1s2s$ ^{3}S, -64.41 eV) [38] are indicated, as well as the KS EXX $1s_\uparrow$, $1s_\downarrow$, and $2s_\uparrow$ spin-orbital energies (-55.94 eV, -67.18 eV, and -5.342 eV, respectively) [39] and the exact KS $1s_\uparrow$ orbital energy (-55.97 eV [39]).
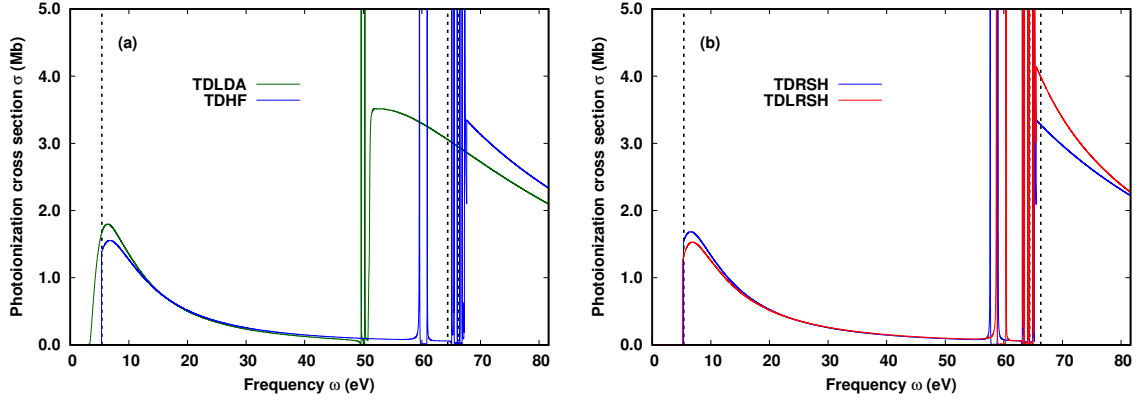

FIG. 2. Photoionization cross section of the Li atom calculated by (a) TDLDA and TDHF, and by (b) TDRSH and TDLRSH (using the optimal adimensional range-separation parameters determined in Section III A, i.e. $\tilde{\mu}_{RSH}$ = 1.431 for TDRSH and $\tilde{\mu}_{LRSH}$ = 0.560 for TDLRSH). The vertical dashed lines correspond to the experimental IP (5.392 eV) [37] and the $1s_\downarrow$ and $1s_\uparrow$ ionization edges (64.41 and 66.31 eV, respectively) [38].

TDLRSH photoionization spectra display a series of core resonances. In comparison to TDRSH, TDLRSH gives smaller cross sections in the 2s continuum region (near 5 eV) and larger cross sections in the 1s continuum region (near 70 eV).

C. Core resonances

Figure 3 shows the TDLDA, TDHF, TDRSH, and TDLRSH photoionization spectra in the energy region of the core (Feshbach-type) resonances $1s_\uparrow \rightarrow np_\uparrow$ and $1s_\downarrow \rightarrow np_\downarrow$. In all cases, the cross section follows a characteristic asymmetric Fano lineshape which can be fitted to the analytical expression [19, 46]

$$\sigma = \sigma_0(1 + a\epsilon)\left[\rho^2 \frac{(q + \epsilon)^2}{1 + \epsilon^2} - \rho^2 + 1\right], \qquad (27)$$

where $\epsilon = 2(\omega - E_R)/\Gamma$. Here, E_R is the resonance energy, Γ is the resonance width (or inverse lifetime), q is the asymmetry Fano parameter, σ_0 is the total background cross section, a is a coefficient for the total background linear drift, and ρ^2 is the ratio between the background cross section for transitions to continuum states that interact with the discrete resonant state and the total background cross section. The fitted parameters for the $1s_\uparrow \rightarrow 2p_\uparrow$, $1s_\downarrow \rightarrow 2p_\downarrow$, $1s_\uparrow \rightarrow 3p_\uparrow$, $1s_\uparrow \rightarrow 3p_\uparrow$, and $1s_\uparrow \rightarrow 3p_\uparrow$ resonances are given in Table III C. For the fitting procedure, the cross section at the resonance energy $\sigma(E_R)$ was included in the data as the asymmetry parameter q is very sensitive to the value of the cross section at the peak. To attribute the correct spin to each resonance line, for each method, we have just calculated photoionization spectra with uncoupled spin-$\uparrow$ and spin-$\downarrow$ excitations (not shown), giving resonances with definite spin which are very close to the original ones.

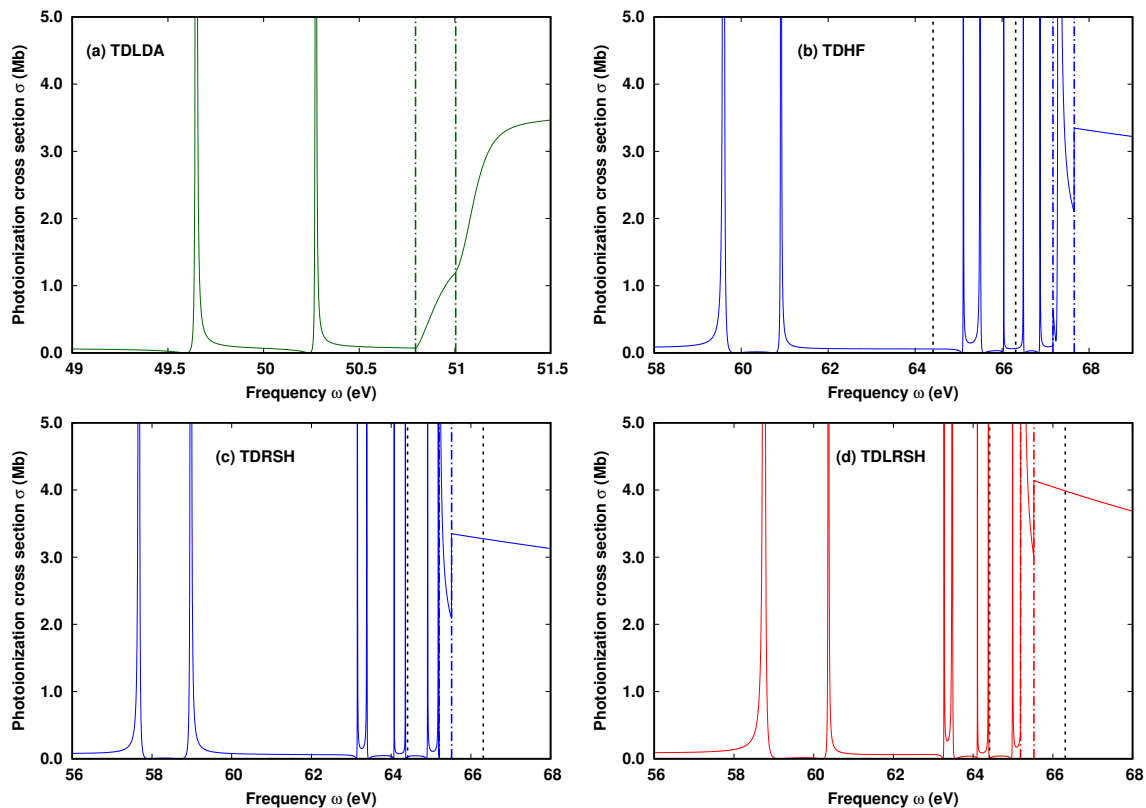As references, we have included in Table III C, the experi-

FIG. 3. Core resonance $1s_\uparrow \to np_\uparrow$ and $1s_\downarrow \to np_\downarrow$ of the Li atom calculated by (a) TDLDA, (b) TDHF, (c) TDRSH, and (d) TDLRSH (using the optimal adimensional range-separation parameters determined in Section III A, i.e. $\tilde{\mu}_{RSH} = 1.431$ for TDRSH and $\tilde{\mu}_{LRSH} = 0.560$ for TDLRSH). The vertical dash-dotted colored lines correspond the $1s_\downarrow$ and $1s_\uparrow$ ionization edges of the method considered, and the vertical dashed black lines correspond to the experimental $1s_\downarrow$ and $1s_\uparrow$ ionization edges (64.41 and 66.31 eV, respectively) [38].

mental resonance energies [47], as well as accurate results obtained with the R-matrix method [48, 49] and the saddle-point complex-rotation (SPCR) method [50, 51]. The first core resonance cross-section profiles obtained with the R-matrix can be found in Fig. 1a of Ref. 49.

The TDLDA $1s_\uparrow \to 2p_\uparrow$ and $1s_\downarrow \to 2p_\downarrow$ resonances occur at much too low energies (by 9.3 eV and 10.1 eV, respectively). With TDHF, the $1s_\uparrow \to 2p_\uparrow$ and $1s_\downarrow \to 2p_\downarrow$ resonances have slightly too high energies (by 0.7 eV and 0.5 eV, respectively) and the errors increase for the $1s_\downarrow \to 3p_\downarrow$ and $1s_\uparrow \to 3p_\uparrow$ resonances (with energies overestimated by 2.7 eV and 1.4 eV, respectively). TDRSH does not systematically improve over TDHF: although TDRSH gives $1s_\downarrow \to 3p_\downarrow$ and $1s_\uparrow \to 3p_\uparrow$ resonance energies with much smaller absolute errors (0.7 eV for both resonances) compared to TDHF, it gives $1s_\uparrow \to 2p_\uparrow$ and $1s_\downarrow \to 2p_\downarrow$ resonance energies with larger absolute errors (1.2 eV and 1.4 eV, respectively). By contrast, TDLRSH provides a systematic improvement over TDHF: it gives $1s_\uparrow \to 2p_\uparrow$ and $1s_\downarrow \to 2p_\downarrow$ resonance energies with absolute errors of 0.15 eV and 0.02 eV, respectively, and $1s_\downarrow \to 3p_\downarrow$ and $1s_\uparrow \to 3p_\uparrow$ resonance energies with absolute errors of 0.9 eV and 0.6 eV, respectively.

The resonance widths Γ and Fano asymmetric parameters q, which determined the shape of the resonances, are very sensitive to the method employed. The resonance widths Γ

should correspond to the decay rate of the core resonances through the Auger process $1s2snp \to 1s^2 + e$ (for $n = 2$ or 3). Since the last configuration is a single excitation with respect to the ground-state configuration, one can a priori hope to obtain reasonable resonance widths with the present adiabatic TDDFT/TDHF-type methods (in contrast with the situation of the core resonances of the Be atom with Auger decays involving a double excitation [17]). While TDLDA turns out to give much too small widths Γ (by one or two orders of magnitude) for the first two core resonances, TDHF gives indeed reasonable widths Γ (of the correct order of magnitude) for the $1s_\uparrow \to 2p_\uparrow$, $1s_\downarrow \to 3p_\downarrow$, and $1s_\uparrow \to 3p_\uparrow$ resonances. TDHF only largely underestimates (by about a factor 50) the width of the $1s_\downarrow \to 2p_\downarrow$ resonance. According to the reference methods, this last resonance has much larger decay rate than the other resonances considered here, with could be explained by a larger proximity of the two electrons involved in the Auger process in the $1s (2s2p)^1P$ resonance state [52]. This particular feature of the $1s (2s2p)^1P$ resonance state is not reproduced by TDHF. As regards now TDRSH and TDLRSH, they give resonance widths of the same order of magnitude than the TDHF ones, sometimes smaller and sometimes larger, without any clear pattern emerging.

TABLE I. Resonance energy E_R, resonance width Γ, Fano asymmetric parameter q, total background cross section σ_0, background ratio parameter ρ^2, background linear drift a, and maximum value of the cross section at the resonance energy $\sigma(E_R)$ for the $1s_\uparrow \to 2p_\uparrow$, $1s_\downarrow \to 2p_\downarrow$, $1s_\uparrow \to 3p_\uparrow$, $1s_\uparrow \to 3p_\uparrow$, and $1s_\uparrow \to 3p_\uparrow$ core resonances of the Li atom calculated by TDLDA, TDHF, TDRSH, and TDLRSH (using the optimal adimensional range-separation parameters determined in Section III A, i.e. $\tilde{\mu} = 1.431$ for TDRSH and $\tilde{\mu} = 0.560$ for TDLRSH). As references, we also report experimental values and accurate results from R-matrix and SPCR calculations.

	E_R (eV)	Γ (meV)	q	σ_0 (Mb)	ρ^2	a	$\sigma(E_R)$ (Mb)
resonance $1s_\uparrow \to 2p_\uparrow$ [configuration $1s\,(2s2p)^3P$]							
TDLDA	49.648	0.279	403.52	0.061	1.0072	$-4.88 \cdot 10^{-5}$	10047.3
TDHF	59.595	5.618	-93.67	0.051	1.0448	$-4.96 \cdot 10^{-4}$	469.2
TDRSH	57.672	2.874	-170.78	0.045	1.0074	$-3.66 \cdot 10^{-4}$	1326.5
TDLRSH	58.756	5.439	-136.31	0.055	1.0288	$-3.33 \cdot 10^{-4}$	1060.5
R-matrix[a]	58.916	3.48					
R-matrix[b]	58.898	3.99					
SPCR[c]	58.910	3.33					5164
Experiment[d]	58.909						
resonance $1s_\downarrow \to 2p_\downarrow$ [configuration $1s\,(2s2p)^1P$]							
TDLDA	50.273	0.142	488.14	0.076	1	$-2.76 \cdot 10^{-5}$	18162.4
TDHF	60.915	0.174	1692.39	0.042	1.0054	$1.86 \cdot 10^{-5}$	121319.2
TDRSH	58.974	0.566	891.62	0.042	1.0443	$5.83 \cdot 10^{-5}$	34676.3
TDLRSH	60.370	0.273	1132.04	0.039	1.0160	$4.12 \cdot 10^{-5}$	50323.1
R-matrix[a]	60.409	9.54					
R-matrix[b]	60.357	10.52					
SPCR[c]	60.398	9.56					84.3
Experiment[d]	60.392						
resonance $1s_\downarrow \to 3p_\downarrow$ [configuration $(1s2s)^3S\,3p$]							
TDHF	65.109	0.454	149.05	0.083	1	$1.52 \cdot 10^{-4}$	1824.0
TDRSH	63.155	0.410	128.83	0.077	1	$4.15 \cdot 10^{-4}$	1268.7
TDLRSH	63.272	0.675	79.74	0.106	1	$1.33 \cdot 10^{-3}$	671.8
R-matrix[a]	62.423	0.196					
R-matrix[b]	62.415	0.214					
SPCR[c]	62.417	0.203					14630
Experiment[d]	62.417						
resonance $1s_\uparrow \to 3p_\uparrow$ [configuration $(1s2s)^1S\,3p$]							
TDHF	65.495	0.580	-276.35	0.062	1	$-2.54 \cdot 10^{-4}$	4741.2
TDRSH	63.391	0.156	-546.66	0.066	1	$-1.23 \cdot 10^{-4}$	19821.8
TDLRSH	63.476	0.488	-683.20	0.016	1	$-3.58 \cdot 10^{-3}$	7372.2
R-matrix[a]	64.051	0.352					
SPCR[c]	64.050	0.391					173
Experiment[d]	64.052						

[a]From Ref. 48.

[b]From Ref. 49.

[c]From Ref. 50 (see also Ref. 51).

[d]From Ref. 47.

IV. CONCLUSION

In this work, we have considered the calculation of photoionization spectra of open-shell systems using two variants of range-separated TDDFT, namely, TDRSH, which uses a global range-separation parameter, and TDLRSH, which uses a local range-separation parameter, and compared with standard TDLDA and TDHF. For this, we have formulated

a spin-unrestricted linear-response Sternheimer approach in a non-orthogonal B-spline basis set and using appropriate frequency-dependent boundary conditions. We have illustrated this approach on the photoionization spectrum of the Li atom, focusing in particular on the core resonances.

TDRSH and TDLRSH provide a big improvement over TDLDA and a small improvement over TDHF. Moreover, TDLRSH tends to provide slightly more accurate resonance energies than TDRSH. This suggests that TDRSH and TDLRSH are adequate simple methods for estimating single-electron photoionization spectra of open-shell systems, even though neither TDRSH or TDLRSH can compete with more accurate methods such as the R-matrix and SPCR methods, especially for the calculation of resonance widths.

To extend this work to general molecular systems, the present linear-response Sternheimer approach could be implemented with Gaussian basis sets and should be extended from spherical boundary conditions to general nonlocal Robin boundary conditions. To improve the accuracy, the present approach could be extended to range-separated multiconfiguration TDDFT [11].

AUTHOR DECLARATIONS

The authors have no conflicts to disclose.

DATA AVAILABILITY

The data that support the findings of this study are available from the corresponding author upon reasonable request.

[1] E. Runge and E. K. U. Gross, Phys. Rev. Lett. **52**, 997 (1984).

[2] E. K. U. Gross and W. Kohn, Phys. Rev. Lett. **55**, 2850 (1985).

[3] M. E. Casida, in *Recent Advances in Density Functional Methods, Part I*, edited by D. P. Chong (World Scientific, Singapore, 1995), p. 155.

[4] M. Petersilka, U. J. Gossmann and E. K. U. Gross, Phys. Rev. Lett. **76**, 1212 (1996).

[5] Y. Tawada, T. Tsuneda, S. Yanagisawa, T. Yanai and K. Hirao, J. Chem. Phys. **120**, 8425 (2004).

[6] T. Yanai, D. P. Tew and N. C. Handy, Chem. Phys. Lett. **393**, 51 (2004).

[7] M. J. G. Peach, T. Helgaker, P. Salek, T. W. Keal, O. B. Lutnæs, D. J. Tozer and N. C. Handy, Phys. Chem. Chem. Phys. **8**, 558 (2006).

[8] E. Livshits and R. Baer, Phys. Chem. Chem. Phys. **9**, 2932 (2007).

[9] R. Baer, E. Livshits and U. Salzner, Annu. Rev. Phys. Chem. **61**, 85 (2010).

[10] T. Tsuneda, J.-W. Song, S. Suzuki and K. Hirao, J. Chem. Phys. **133**, 174101 (2010).

[11] E. Fromager, S. Knecht and H. J. A. Jensen, J. Chem. Phys. **138**, 084101 (2013).

[12] E. Rebolini, A. Savin and J. Toulouse, Mol. Phys. **111**, 1219 (2013).

[13] D. Jacquemin, E. A. Perpète, G. E. Scuseria, I. Ciofini and C. Adamo, J. Chem. Theory Comput. **4**, 123 (2008).

[14] A. D. Laurent and D. Jacquemin, Int. J. Quantum Chem. **113**, 2019 (2013).

[15] F. Zapata, E. Luppi and J. Toulouse, J. Chem. Phys. **150**, 234104 (2019).

[16] J. Toulouse, E. Rebolini, T. Gould, J. F. Dobson, P. Seal and J. G. Ángyán, J. Chem. Phys. **138**, 194106 (2013).

[17] K. Schwinn, F. Zapata, A. Levitt, E. Cancès, E. Luppi and J. Toulouse, J. Chem. Phys. **156**, 224106 (2022).

[18] G. D. Mahan and K. R. Subbaswamy, *Local Density Theory of Polarizability* (Plenum Press, New York, 1990).

[19] M. Stener, P. Decleva and A. Lisini, J. Phys. B, **28**, 4973 (1995).

[20] M. Stener and P. Decleva, J. Chem. Phys. **112**, 10871 (2000).

[21] K. Yabana, T. Nakatsukasa, J.-I. Iwata and G. F. Bertsch, Phys. Stat. Sol. **243**, 1121 (2006).

[22] X. Andrade, S. Botti, M. A. L. Marques and A. Rubio, J. Chem. Phys. **126**, 184106 (2007).

[23] D. A. Strubbe, L. Lehtovaara, A. Rubio, M. A. L. Marques and S. G. Louie, in *Fundamentals of Time-Dependent Density Functional Theory, Lecture Notes in Physics Vol. 837*, edited by M. A. Marques, N. T. Maitra, F. M. Nogueira, E. Gross and A. Rubio (Springer, Berlin Heidelberg, 2012), pp. 139–166.

[24] F. Hofmann, I. Schelter and S. Kümmel, J. Chem. Phys. **149**, 024105 (2018).

[25] F. Hofmann, I. Schelter and S. Kümmel, Phys. Rev. A **99**, 022507 (2019).

[26] F. Hofmann and S. Kümmel, J. Chem. Phys. **153**, 114106 (2020).

[27] J. G. Ángyán, I. C. Gerber, A. Savin and J. Toulouse, Phys. Rev. A **72**, 012510 (2005).

[28] A. Savin, in *Recent Developments of Modern Density Functional Theory*, edited by J. M. Seminario (Elsevier, Amsterdam, 1996), pp. 327–357.

[29] S. Paziani, S. Moroni, P. Gori-Giorgi and G. B. Bachelet, Phys. Rev. B **73**, 155111 (2006).

[30] A. V. Krukau, G. E. Scuseria, J. P. Perdew and A. Savin, J. Chem. Phys. **129**, 124103 (2008).

[31] T. Aschebrock and S. Kümmel, J. Chem. Phys. **151**, 154108 (2019).

[32] S. Klawohn and H. Bahmann, J. Chem. Theory Comput. **16**, 953 (2020).

[33] T. M. Maier, Y. Ikabata and H. Nakai, J. Chem. Phys. **154**, 214101 (2021).

[34] M. Brütting, H. Bahmann and S. Kümmel, J. Chem. Phys. **156**, 104109 (2022).

[35] C. de Boor, *A practical Guide to Splines* (Springer Books, 1978).

[36] H. Bachau, E. Cormier, P. Decleva, J. E. Hansen and F. Martin, Rep. Prog. Phys. **64**, 1815 (2001).

[37] A. Kramida, Yu. Ralchenko, J. Reader and and NIST ASD Team, NIST Atomic Spectra Database (ver. 5.9), [Online]. Available: `https://physics.nist.gov/asd` [2021, December 19]. National Institute of Standards and Technology, Gaithersburg, MD. (2021).

[38] B. Langer, J. Viefhaus, O. Hemmers, A. Menzel, R. Wehlitz and U. Becker, Phys. Rev. A. **43**, 1652 (1991).

[39] J. Chen, J. B. Krieger, R. O. Esquivel, M. J. Stott and G. J. Iafrate, Phys. Rev. A. **54**, 1910 (1996).

[40] C.-O. Almbladh and U. von Barth, Phys. Rev. B **31**, 3231 (1985).

[41] O. V. Gritsenko and E. J. Baerends, J. Chem. Phys. **117**, 9154 (2002).

[42] T. Stein, L. Kronik and R. Baer, J. Am. Chem. Soc. **131**, 2818 (2009).

[43] T. Stein, L. Kronik and R. Baer, J. Chem. Phys. **131**, 244119 (2009).

[44] E. Wigner, Phys. Rev. **73**, 1002 (1948).

[45] H. R. Sadeghpour, J. L. Bohn, M. J. Cavagnero, B. D. Esryk, I. I. Fabrikant, J. H. Macek and A. R. P. Rau, J. Phys. B, **33**, R93 (2000).

[46] U. Fano and J. W. Cooper, Phys. Rev. **137**, A1364 (1965).

[47] A. M. Cantù, W. H. Parkinson, G. Tondello and G. P. Tozzi, J. Opt. Soc. Am. **67**, 1030 (1977).

[48] O. Zatsarinny and C. Froese Fischer, J. Phys. B **33**, 313 (2000).

[49] J. Li, J. D. Liu, S. B. Zhang and B. J. Ye, Mod. Phys. Lett. B **30**, 1650204 (2016).

[50] K. T. Chung, Phys. Rev. A. **56**, R3330 (1997).

[51] K. T. Chung, Radiat. Phys. Chem. **70**, 83 (2004).

[52] K. T. Chung, Phys. Rev. A. **59**, 2065 (1999).